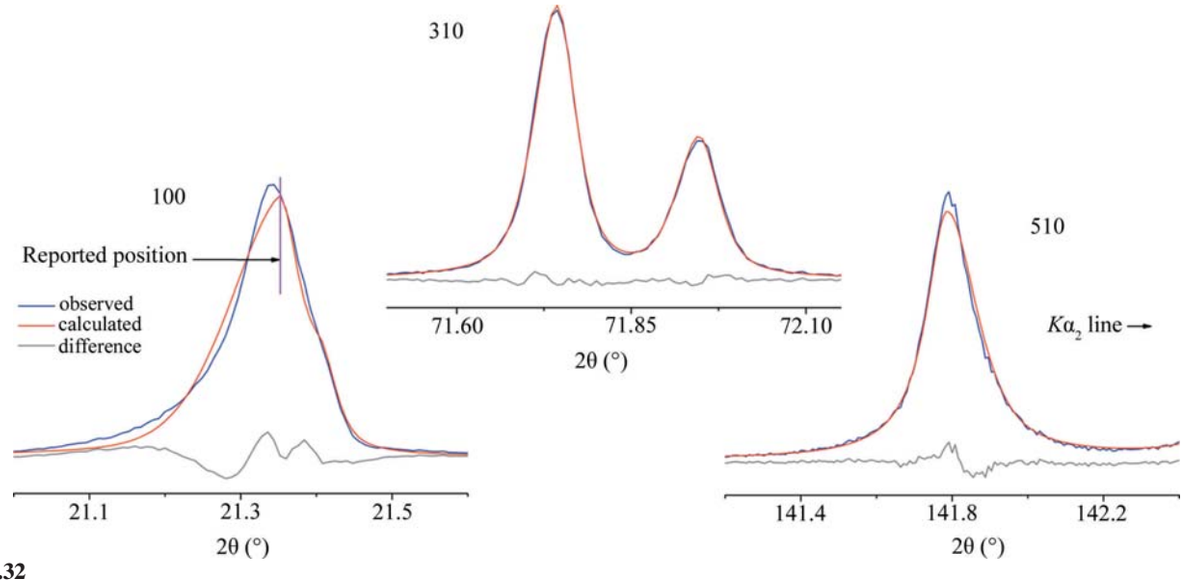

Figure 3.1.32
Fits of the split pseudo-Voigt PSF to the low-angle 100, mid-angle 310 and high-angle 510 lines from SRM 660b illustrating the erroneous peak position and FWHM value reported for the 100 and 510 lines, respectively.

of the same raw data from SRM 660b used to generate Fig. 3.1.26. In general, results from the three commercial codes were in close correspondence. When used on a split PSF, the Caglioti function was applied independently to the left and right FWHM values. A five- to seven-term Chebyshev polynomial was used for modelling the background in these refinements. The goodness of fit (GoF) (which is the square root of reduced χ^2) residual error term of the refinements ranged from 1.6 to 1.9, with the unconstrained refinements yielding the slightly improved fits to the data. Fig. 3.1.32 illustrates the fit quality of typical results using the split pseudo-Voigt PSF. However, as will be demonstrated, the more plausible parameters, particularly in the context of the FWHM values, were often obtained with the more constrained refinements.

The results from the fitting of the Voigt PSF provide a reference for consideration of the $\Delta(2\theta)$ data of Fig. 3.1.29. The use of any of the symmetric PSFs considered here, with or without the Caglioti constraint, resulted in curves virtually identical to the one displayed in Fig. 3.1.29 for the Voigt PSF. Not surprisingly, the symmetric PSF performs quite well in the mid-angle region where the profiles are symmetric but will report an erroneous position in the direction of the asymmetry, when it is present. However, the opposite effect was observed with the use of any of the split PSFs, as can be seen in Figs. 3.1.29 and 3.1.32. When two HWHM values are refined, the larger HWHM value will shift the reported peak position in the direction of the smaller one. This effect can be readily observed in the fit quality of the low-angle 100 reflection displayed in Fig. 3.1.32. The spilt PSFs yield results that reflect an overly asymmetric profile; thus the reported peak positions are displaced to high angle at 2θ angles below 100°, and to low angle at 2θ angles above 100°. Curiously this effect was markedly reduced in one of the commercial computer codes (not shown) and was the sole difference observed between them when the models were equivalent. It is apparent that subtleties in implementation of an ostensibly identical PSF and minimization algorithm (the Marquardt algorithm) can result in dramatic differences in results. Careful examination of the fit quality is required to assess the reliability of profile-fitting results. The data of Fig. 3.1.29 indicate that errors in peak position of up to 0.015° 2θ are plausible with profile fitting of these data with these PSFs. In contrast to its use with symmetric PSFs, the Caglioti function will improve results when using split PSFs (Fig. 3.1.30).

Consideration of the issues related to profile fitting shown in Fig. 3.1.32 led to the conjecture that fitting the data with a uniform weighting as opposed to Poisson statistical weighting might result in more accurate determination of the peak position and FWHM parameters. (In the vast majority of circumstances this approach would never be used, because the integrated intensity is a critical metric.) This was tried, and resulted in considerable success. Fig. 3.1.30 displays data from the use of split pseudo-Voigt that are in very good agreement with second-derivative values.

Experimental and simulated values of the FWHM are displayed in Figs. 3.1.27 and 3.1.31. Data from the profile refinements performed without the use of the Caglioti function, displayed in Figs. 3.1.27 and 3.1.31, yield independently determined measures of the FWHM. Again, the lack of scatter and the continuity of these FWHM values are consistent with proper operation of the instrument, *i.e.* an absence of 'high-frequency' problems. The basic trends are also consistent with the instrument optics: at low 2θ the observed increase in FWHM is due to both the flat specimen and axial divergence aberrations, while at high 2θ angular dispersion dominates and a substantial increase in FWHM with $\tan\theta$ is apparent. The FPA simulations were performed using the settings for high and low resolution. The FWHM values were determined numerically from the simulated patterns; no PSF was used. As shown with the simulated data, the degree of upturn at low 2θ increases with a decrease in instrument resolution and *vice versa*. Angular-dispersion effects, however, are less dependent on the instrument configuration; FWHM values tend towards convergence at high 2θ (Fig. 3.1.27).

As seen in Fig. 3.1.27, above 40° 2θ the Voigt and split-Voigt PSFs give similar values for the FWHM and a fairly accurate representation of instrument performance. It was observed that with regard to the correlation between FWHM values for split *versus* symmetric PSFs, the other PSFs behaved in an analogous manner to the Voigt (not shown): above 40° 2θ the values reported for the FWHM from split *versus* symmetric PSFs are nearly identical. From Fig. 3.1.31, the split Pearson VII PSF underestimates the FWHM throughout the mid-angle region; this error was duplicated with the use of the symmetric Pearson VII